PICOSECOND IMPULSIVE STIMULATED BRILLOUIN SCATTERING: OPTICAL EXCITATION OF COHERENT TRANSVERSE ACOUSTIC WAVES AND APPLICATION TO TIME-DOMAIN INVESTIGATIONS OF STRUCTURAL PHASE TRANSITIONS

Margaret M. ROBINSON, Yong-Xin YAN [1], Edward B. GAMBLE Jr. [2], Leah Ruby WILLIAMS [3], Jeffrey S. METH and Keith A. NELSON
Department of Chemistry, Massachusetts Institute of Technology, Cambridge, Massachusetts 02139, USA

Received 26 October 1984

A practical stimulated Brillouin-scattering method for spectroscopic characterization of low-frequency excitations is extended to permit optical generation and detection of phase-coherent transverse, longitudinal, and mixed polarization acoustic phonons, tunable over a wide frequency range, in solid media. Results are presented for BK-7 glass and the KH_2PO_4 crystal near its structural phase transition (SPT). Time-domain observations of acoustic phonon-induced ordering near SPTs in KH_2PO_4 and KD_2PO_4 were carried out, and applications of the technique to measurements of SPT dynamics are discussed.

1. Introduction

The utility of coherent light-scattering techniques for the study of optic phonons, molecular vibrations, and electronic and other excitations is widely appreciated [1]. Coherent anti-Stokes Raman scattering (CARS) and related methods can offer high sensitivity and spectral resolution, and in many cases can provide information which is difficult to obtain through conventional scattering techniques [1].

Stimulated Brillouin scattering (SBS) involving acoustic phonons [2] could offer similar advantages but has rarely been used due to its technical difficulty. If two laser beams (ω_1, k_1) and (ω_2, k_2) are crossed inside a sample to generate phase-coherent acoustic phonons $(\omega_s = \omega_1 - \omega_2, k_s = k_1 - k_2)$, precise control must be maintained over both the laser frequencies since the phonon frequency is small (typically, $\omega_s/2\pi < 10$ GHz). Moreover, the acoustic-phonon dispersion relation ($\omega_s/k_s = v_s$, where $v_s(k_s)$ is the sound velocity for the mode of interest) places a stringent phase-matching requirement on the experimental geometry. Variation of phonon frequency, polarization, or orientation demands precise readjustment of laser frequencies and/or experimental geometry. Only a handful of successful experiments of this type have been reported [3], in marked contrast to the popularity of CARS-type methods through which higher-frequency, non-dispersive excitations are routinely investigated.

Recently, a time-domain "impulsive" SBS (ISBS) technique which circumvents the technical problems discussed above was introduced and used to investigate longitudinal acoustic phonon properties (velocities, attenuations, and photoelastic constants) in various liquids [4]. It was subsequently predicted that generation of transverse, longitudinal, and mixed-polarization ultrasonic waves in solids and other condensed phases should be possible [5]. Here we report results demonstrating the predicted mode selectivity. The capability for transverse wave excitation and detection is particularly interesting in connection with many structural phase transitions in which the low-symmetry phase can be characterized by shear acoustic strain (i.e. in

[1] Also at: Department of Physics, Massachusetts Institute of Technology, Cambridge, Massachusetts 02139, USA.
[2] Also at: Department of Electrical Engineering and Computer Science, Massachusetts Institute of Technology, Cambridge, Massachusetts 02139, USA.
[3] AT&T Bell Laboratories Scholar.

0 009-2614/84/$ 03.00

which shear strain is an order parameter [6]. The ISBS technique permits time-resolved observations of acoustic phonon-induced ordering near such transitions. We report preliminary time-resolved ISBS results near the ferroelectric transitions in KH_2PO_4 (KDP) [7] and KD_2PO_4(KD*P) [8] and discuss appplications of ISBS to measurements of structural phase transition dynamics.

We note that a related, less mode-selective technique for optical generation of longitudinal and mixed-polarization acoustic waves via light absorption and impulsive heating has been reported and applied to crystals and other condensed phases [4,9,10]. Pure transverse waves cannot be excited by impulsive heating

2. The method

The picosecond ISBS technique is illustrated in fig. 1. Two *temporally short* laser pulses centered at the *same* frequency, (ω, k_1) and (ω, k_2), are overlapped spatially and temporally inside the sample to excite

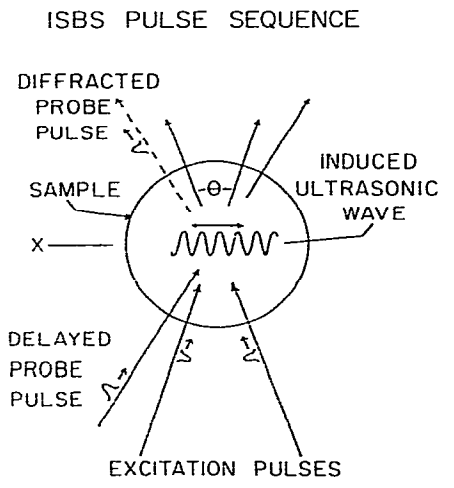

Fig. 1. Schematic illustration of the impulsive stimulated Brillouin-scattering experiment. The crossed excitation pulses generate coherent, counterpropagating acoustic phonons, forming an ultrasonic standing wave which coherently scatters (diffracts) the delayed probe pulse. The acoustic-wave polarization is controlled by the excitation-pulse polarizations (see text). The acoustic wavevector is given by the wavevector difference of the excitation pulses

coherent, counterpropagating acoustic phonons of the difference wavevector $k_s = \pm(k_1 - k_2)$ through SBS. The excitation pulse duration must be *shorter* than the phonon oscillation period $2\pi/\omega_s$ so that the acoustic mode is driven *impulsively*. The acoustic frequency $\omega_s = |k_s| v_s$ is derived from the *inherent spectral width* of the picosecond excitation pulses. The coherent phonons $(\omega_s, \pm k_s)$ form an ultrasonic standing wave in the scattering volume. To describe the acoustic standing-wave displacements, we define a coordinate system in which the excitation pulses propagate in the xz ("horizontal") plane with their angle of intersection bisected by the z-axis. The acoustic wavevector then lies along the x-axis, as in fig. 1. Assuming this is a pure acoustic-mode direction, the acoustic strain is [5]

$$S_{xi}(x, t) = \frac{k_s n^3 p I}{v_s \rho c} \exp(-\gamma_s t) \cos(k_s x) \sin(\omega_s t) , \quad (1)$$

where n is the refractive index, p the photoelastic constant, I the integrated energy flux of each excitation pulse, ρ the density, c the speed of light in air, and γ_s the acoustic attenuation constant. In eq. (1), the appropriate elements of tensor quantities n and p must be used. These depend on the excitation pulse polarizations (see below). Eq. (1) describes the acoustic standing-wave displacements whose amplitude depends on the laser intensity and material parameters.

The acoustic-wave polarization is controlled by the polarizations of the excitation pulses [5]. For example, a longitudinal wave can be produced with two vertically polarized excitation pulses. (The strain component is S_{xx} and the photoelastic constant is p_{12}.) With one excitation pulse horizontally polarized and the other vertically polarized, a transverse wave is generated. (Strain is S_{xy} and photoelastic constant is p_{66}.) These cases are just the stimulated analogs of thermal V–V and V–H Brillouin scattering from longitudinal and transverse phonons, respectively. The acoustic wavevector can be varied by changing the excitation geometry or wavelength. Thus the acoustic-wave orientation can be controlled and the frequency can be continuously tuned over a very wide range (about 3 MHz–30 GHz in most materials, with excitation pulses derived from a Nd:YAG laser and harmonics).

The ultrasonic standing wave is detected by time-resolved coherent scattering, i.e. Bragg diffraction, of variably delayed picosecond probe pulses (see fig. 1).

The diffraction efficiency depends on the square of the phonon-induced peak-to-null variation in refractive index, given by

$$n_1(t) = -\tfrac{1}{2} p n^3 S(t) . \quad (2)$$

Assuming the probe pulse enters the ultrasonic "volume grating" at the Bragg angle, θ_p, the diffraction efficiency is given by [4]

$$D(t) = \sin^2 [\pi n_1(t) L/\lambda_p \cos\theta_p] \approx [\pi n_1(t) L/\lambda_p]^2$$

$$= [(\pi n^6 k_s p^2 IL/\lambda_p v_s \rho c) \exp(-\gamma_s t) \sin(\omega_s t)]^2 \quad (3)$$

for small D_{max} and θ_p; L is the effective grating thickness [11]. Eq. (3) shows that time-dependent diffracted signal oscillates at twice the standing-wave frequency and decays at twice the acoustic attenuation rate.

We discuss below experiments carried out on KDP and KD*P near their ferroelectric phase transitions. In both materials, the x-propagating, y-polarized transverse acoustic mode "softens" near the transition temperature, T_c. The low-frequency elastic constant, $c_{66} = v_s^2 \rho$, decreases as $T \to T_c^+$ as [12]

$$c_{66}^E = c_{66}^P - a_{36}^2 \epsilon_{33}^S / 4\pi = c_{66}^P - a_{36}^2 C/4\pi(T - T_0) , \quad (4)$$

while the low-frequency photoelastic constant diverges as [13]

$$p_{66}^E = p_{66}^P + \rho_{36}^S a_{36} \epsilon_{33}^S / 4\pi = p_{66}^P + \rho_{36}^S a_{36} C/4\pi(T - T_0), \quad (5)$$

where the superscripts E, P, and S indicate constant electric field, polarization, and strain, respectively; a_{36} is the piezoelectric stress constant, ϵ_{33} the dielectric constant, C the Curie constant, T_0 the clamped transition temperature and ρ_{36} the electro-optic constant. In the ISBS experiment, the wavevector k_s is fixed by the experimental geometry while ω_s, v_s, and p vary with temperature near T_c. (The attenuation rate γ_s also increases near T_c, but this divergence is not discussed in detail below.) Eq. (3) shows that ISBS signal from a soft acoustic mode should change in several ways near T_c. First, the frequency of the time-dependent oscillations in the signal should decrease as ω_s decreases. Second, the intensity of diffracted signal, which depends on p_{66}^4/c_{66}, should increase dramatically. Finally, the time-dependent decay rate of signal due to acoustic attenuation should increase. Similar effects can be observed in conventional Brillouin scattering [12,13] as the frequency shift of scattered light decreases near T_c, the linewidth broadens, and the intensity increases as p_{66}^2/c_{66}. Some advantages of the ISBS experiment for SPT study are discussed below.

3. Experimental

The laser is a continuously pumped, acousto-optically Q-switched and mode-locked Nd:YAG system which produces 1.06 μm, 2 mJ pulse trains consisting of about 30 mode-locked pulses (85 ps in duration) at a repetition rate of 500 Hz. Three pulses of 80 μJ each were selected by electro-optic Pockels' cells with avalanche transistor drivers. Two of the pulses were focused to 270 μm spot sizes and overlapped spatially and temporally in the sample to provide the two 1.06 μm excitation pulses. The third pulse was frequency-doubled, variably delayed along a motorized precision delay line, and focused to a 270 μm spot size to provide the 532 nm probe pulse. Diffracted signal was measured with a PIN photodiode and a lock-in amplifier. A similar laser system and experimental arrangement have been described previously [4].

The data to be discussed were taken from commercially obtained, optically polished samples of BK-7 glass, KDP, and KD*P crystals. Alignment of the acoustic wave vector along the crystallographic axes was optimized near T_c by rotating the crystals around both axes perpendicular to the wave vector and finding the orientation which gave the lowest sound velocity. We estimate ±1° angular uncertainty in wave vector alignment. Temperature was controlled to ±0.02 K (short-term) by a commercial closed-cycle refrigerator with a regulated heater. The very strong signals near T_c permitted data to be recorded in about 2 min with minimal temperature fluctuations.

4. Results and discussion

ISBS data from BK-7 glass is shown in fig. 2. Fig. 2a shows longitudinal-wave data taken with parallel-polarized (V—V) excitation pulses. The incident probe pulse and the diffracted signal were V-polarized as well. The frequency measured from the data (±1%) and the wave vector determined by measurement of the experimental geometry (±1%) yield a longitudinal sound velocity $v_s = 6.07 \times 10^5$ cm/s (±2%), in good agreement with

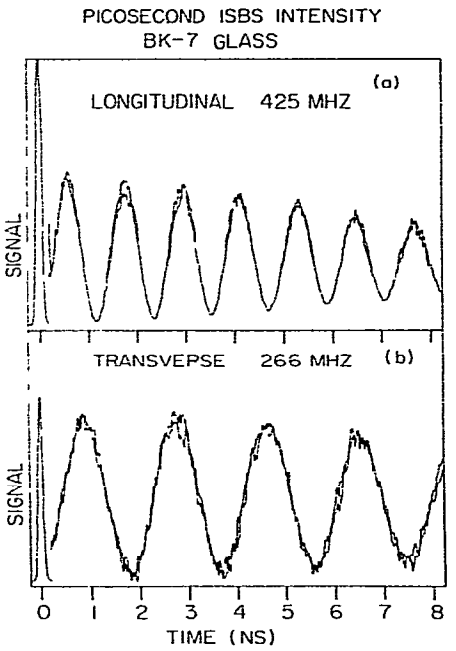

Fig. 2. ISBS data from BK-7 glass. The 1.06 μm excitation pulses were crossed with angle $\theta = 0.0741$ rad (4.25°) ±1% between them. This resulted in an acoustic wavevector $k_S = 4.39 \times 10^3$ cm^{-1} (acoustic wavelength $\Lambda = 14.3$ μm). Each sweep consists of about 100000 excitation–probe repetitions with the 532 nm probe pulse variably delayed relative to the excitation pulses. Two sweeps are shown in each figure to illustrate the reproducibility of the data. (a) Parallel-polarized (V–V) excitation pulses generate a longitudinal acoustic wave. The measured frequency and wavevector yield a speed of sound $v_S = 6.07 \times 10^5$ cm/s ±2%. Maximum diffraction efficiency after $t = 0$ was $D_{max} = 6.3 \times 10^{-8}$ ± 10%. (b) Perpendicularly (V and H) polarized excitation pulses generate a transverse ultrasonic wave with $v_S = 3.81 \times 10^5$ cm/s ±2%; $D_{max} = 1.1 \times 10^{-9}$ ± 10%. The shear-wave polarization is confirmed by the frequency and also by the observation that the polarization of diffracted signal is rotated 90° from that of the incident V-polarized probe pulse. The polarization of light diffracted by the longitudinal wave is not rotated. Excitation conditions other than polarizations were identical. The $t = 0$ spikes, actually about 1000 × stronger than shown, are due to four-wave mixing processes which occur only while all three pulses are coincident in the sample.

literature values [14]. Fig. 2b shows transverse-wave data taken under identical excitation conditions except for the rotation of a single half-wave plate to give perpendicularly (V and H) polarized excitation pulses. The incident probe pulse was again V-polarized, but in this case the diffracted signal was H-polarized. The data yield a transverse sound velocity $v_S = 3.81 \times 10^5$ cm/s (±2%), again in good agreement with earlier results [14]. These results confirm the predicted ISBS mode-selectivity for pure transverse and longitudinal waves [5]. Mixed-polarization waves have also been generated and detected in many crystalline samples.

Measurement of the absolute diffraction efficiencies permits calculation of the photoelastic constants, using the BK-7 parameters [14] $n = 1.5$ and $\rho = 2.5$ g/cm^3. Our results give $p_{12} = 0.26$ and $p_{44} = 0.063$ (±10%), in good agreement with literature values [14]. We have neglected dispersion in n and p due to the uncertainties in our results and in those reported earlier [14]. Acoustic attenuation in BK-7 is too slow to be observed on this time scale. The non-exponential decay in the data, as well as the rise in "baseline", are experimental artifacts due to the acoustic waves propagating out of the excitation volume. These effects can be easily calculated by considering the Gaussian intensity profiles and spot sizes of the excitation and probe pulses, and can be eliminated by using sufficiently large excitation spot sizes. The effects are pronounced in fig. 2a because of the high longitudinal wave velocity.

The nearly second-order structural phase transition (SPT) in KDP between a paraelectric high-T phase and a ferroelectric low-T phase was chosen to illustrate the utility of ISBS for SPT study since the elastic and photoelastic properties of KDP near the transition temperature ($T_c = 122$ K) have been documented [12,13,15]. Coupling between the c_{66} shear acoustic mode and the optic phonon-polarization mode lead to softening of the c_{66} elastic constant near T_c as described by eq. (4) [12]. Fig. 3 shows KDP transverse-wave ISBS data recorded at several temperatures. We observe the expected decrease in sound velocity as $T \to T_c$. We also observe a dramatic rise in the signal intensity, by a factor of over 10000, as shown in fig. 4. The signal intensity, which depends on p_{66}^4/c_{66}, diverges as predicted by eqs. (3)–(5) with the known KDP parameters [12, 13]. The divergence of the p_{66} photoelastic constant occurs due to the linear couplings among strain, electric polarization (the order parameter in this transition), and refractive index. Strain-induced changes in polarization, which increase in magnitude near T_c because the polarization susceptibility ϵ_{33} diverges, modulate the refractive index sharply to produce intense diffraction. *We thus observe acoustically driven dynamic*

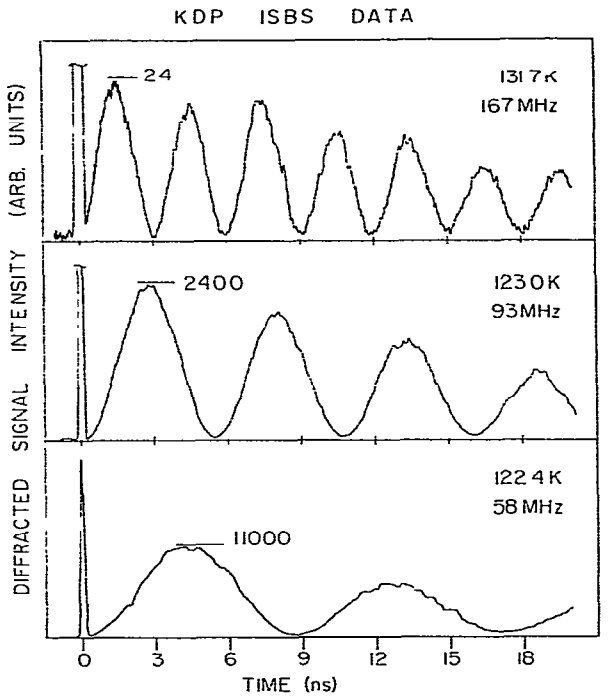

Fig. 3. Temperature-dependent ISBS data from the x-propagating, y-polarized "soft" transverse acoustic mode in KDP near the phase transition temperature T_c = 122.00 K. Excitation and probe conditions were as in fig. 2b except excitation angle $\theta = 7.06°$ giving wave vector $k = 7.27 \times 10^3$ cm^{-1} (acoustic wavelength $\Lambda = 8.64$ μm). As $T \to T_c$, the acoustic velocity decreases and the intensity of coherently scattered signal increases to 11000 times its room-temperature value. The absolute diffraction efficiency in the bottom trace is about 1%. The increase in signal near T_c occurs because acoustic strain induces an electric polarization which couples strongly to the refractive index. Acoustically induced ordering is thus monitored in the time domain. Similar results were observed in KD*P near its ferroelectric transition.

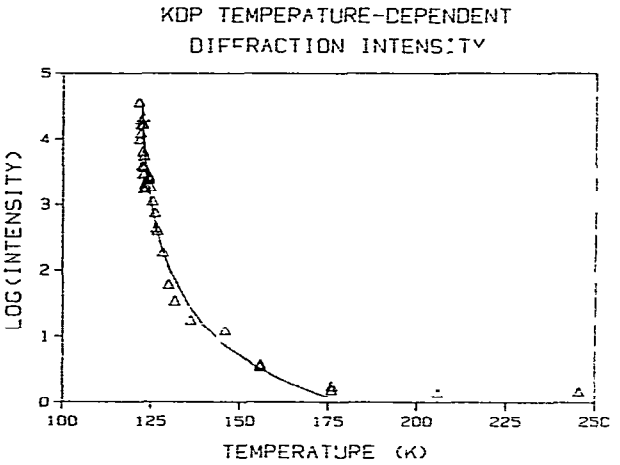

Fig. 4. Temperature-dependent ISBS intensity in KDP. The triangles represent experimental measurements of diffraction intensity from data like those in fig. 3. The solid curve gives the temperature dependence of p_{66}/c_{66}, calculated using eqs. (4) and (5) with KDP parameters that closely describe the experimentally measured temperature dependences of p_{66} and c_{66} over a wide temperature range [12,13]. The 11000-fold increase in signal near T_c is clearly in accordance with eq. (3) and the known properties of KDP near its ferroelastic phase transition.

ordering near SPTs in the time domain. Preliminary ISBS experiments on KD*P near its ferroelectric transition at 220 K, using the same experimental geometry as in the KDP work, have shown a similar softening of the c_{66} shear-wave velocity and dramatic increase in signal intensity as $T \to T_c$.

It is interesting to compare our results with those of conventional Brillouin scattering (BS) and ultrasonics experiments. Ultrasonics work typically probes the 10–50 MHz frequency range. Conventional BS usually is done at near-90° scattering angles to minimize parasitic elastically scattered light, and so probes higher ($\gtrsim$1 GHz) frequencies. In KDP the softening of c_{66} near T_c is observed in both ultrasonics [15] and BS [12,13] experiments, and the BS intensity diverges [12] as p_{66}^2/c_{66}. In KD*P, on the other hand, softening of c_{66} is observed in ultrasonic work [16] but *not* in BS at large angles [8,17], and the BS intensity does not diverge. This indicates that at GHz acoustic frequencies, the order parameter in KD*P cannot follow the acoustic strain. The observation of softening at ultrasonic frequencies indicates order parameter relaxation at intermediate frequencies near T_c. This is confirmed by ultrasonic attenuation measurements as well [16], although due to the strength of attenuation near T_c these measurements were possible only at very low frequencies with an applied dc electric field. Preliminary ISBS results on KD*P were obtained at a sufficiently small scattering angle that softening of c_{66} and divergence of p_{66} were observed. An angle-dependent study is under way and should permit direct determination of the temperature-dependent order parameter relaxation time.

The results obtained thus far illustrate some of the useful features of ISBS for SPT study. First, the wide frequency range accessible to ISBS includes and "connects" the ranges usually explored ultrasonically and in BS. ISBS is not frustrated by strong attenuation and so permits characterization of acoustic properties and order parameter responses at low and high frequencies even very near T_c. Finally, ISBS can resolve low-frequency soft modes which are often obscured by strong parasitic and inherent quasielastic scattering in BS. These features should prove valuable for measurements of SPT dynamics in the MHz–GHz regime, for example in some organic molecular crystals [18] and at incommensurate transitions [19].

In summary, we have demonstrated mode-selective ISBS in solids and illustrated its potential for investigation of SPT dynamics. Time-domain observations of acoustically induced ordering near SPTs have been carried out. In this regard, we mention that ISBS excitation could be followed by measurements of not only diffraction but also birefringence, second-harmonic generation, absorption spectra [9] or other optical properties which may be more sensitive to or provide more direct information about particular types of coupled motion. Finally, the impulsive stimulated scattering (ISS) technique can be extended to permit excitation and characterization of other low-frequency excitations such as optic phonons, phasons and magnons. By using femtosecond pulses, coherent optic phonons with energies up to $\approx 100\ cm^{-1}$ were recently excited and probed [20]. This permitted femtosecond time-resolved CARS without the need for synchronization of two femtosecond lasers of different frequencies. It also suggested possible applications of ISS in ultrahigh-frequency (>1 THz) signal generation.

Acknowledgement

This work was supported in part through National Science Foundation Grant No. DMR-8306701 (MMR and Y-XY), US Army Research Office Contract No. DAAG29-83-K0003 (EBG), and a grant from Research Corporation.

References

[1] M.S. Feld and V.S. Letokhov, eds., Coherent nonlinear optics: recent advances (Springer, Berlin, 1980).
A. Lauberau and W. Kaiser, Rev. Mod. Phys. 50 (1978) 607;
S.D. Durbin, S. M. Arakelian and Y.R. Shen, Phys. Rev. Letters 47 (1981) 1411.
[2] Y.R Shen and N. Bloembergen, Phys. Rev. A137 (1965) 1787;
A. Yariv, IEEE J. Quant. Electron. QE-1 (1965) 28.
[3] A.G. Jacobson and Y.R. Shen, Appl. Phys. Letters 34 (1979) 464;
A. Korpel, R. Adler and B. Alpiner, Appl. Phys Letters 5 (1964) 86;
D.E. Caddes, C.F. Quates and C.D.W. Wilkinson, Appl. Phys. Letters 8 (1966) 309.
[4] K.A. Nelson, R.J.D. Miller and M.D. Fayer, J. Appl. Phys. 53 (1982) 1144;
R.J.D. Miller, R. Casalegno, K.A. Nelson and M.D. Fayer, Chem. Phys. 72 (1982) 371.
[5] K.A. Nelson, J. Appl. Phys. 53 (1982) 6060.
[6] R.A. Cowley, Phys. Rev. B13 (1976) 4877.
[7] E. Courtens and R. Gammon, Ferroelectrics 24 (1980) 19.
[8] R.L. Reese, I.J. Fritz and H.Z. Cummins, Phys. Rev. B7 (1973) 4165.
[9] K.A. Nelson and M.D. Fayer, J. Chem. Phys 72 (1980) 5202.
[10] G. Eyring and M.D. Fayer, Biophys. J. (1984), to be published.
[11] A.E. Siegman, J. Opt. Soc. Am. 67 (1977) 545.
[12] E.M. Brody and H.Z. Cummins, Phys. Rev. B9 (1974) 179.
[13] E.M. Brody and H.Z. Cummins, Phys. Rev. Letters 23 (1969) 1039.
[14] D. Heiman, D.S Hamilton and R.W. Hellwarth, Phys. Rev. B19 (1979) 6583;
V.C. Schaefer and H. Nassenstein, Z. Naturforsch. 8a (1953) 90.
[15] E. Litov and C.W. Garland, Phys. Rev. B2 (1970) 4597;
C.W. Garland and D.B. Novotny, Phys. Rev. 177 (1969) 971.
[16] E. Litov and E.A. Uehling, Phys. Rev. Letters 21 (1968) 809.
[17] M. Sawafuji, M. Tokunaga and I. Tatsuzaki, J. Phys. Soc. Japan 47 (1979) 1860, 1870.
[18] J.F. Scott, G.E. Feldkamp, G.V. Kozlov and A.A. Volkov, Ferroelectrics 52 (1983) 211.
[19] P.W. Young and J.F. Scott, Ferroelectrics 52 (1983) 35.
[20] S. de Silvestri, E.P. Ippen, L.R. Williams, E.B. Gamble Jr. and K.A. Nelson, submitted for publication.